ARCHIVIO ISTITUZIONALE
DELLA RICERCA

Alma Mater Studiorum Università di Bologna
Archivio istituzionale della ricerca

Addressing the Frenkel and charge transfer character of exciton states with a model Hamiltonian based on dimer calculations: Application to large aggregates of perylene bisimide

This is the final peer-reviewed author's accepted manuscript (postprint) of the following publication:

Published Version:
Canola S., Bagnara G., Dai Y., Ricci G., Calzolari A., Negri F. (2021). Addressing the Frenkel and charge transfer character of exciton states with a model Hamiltonian based on dimer calculations: Application to large aggregates of perylene bisimide. THE JOURNAL OF CHEMICAL PHYSICS, 154(12), 1-13 [10.1063/5.0045913].

Availability:
This version is available at: https://hdl.handle.net/11585/818062 since: 2021-04-06

Published:

DOI: http://doi.org/10.1063/5.0045913

Terms of use:

Some rights reserved. The terms and conditions for the reuse of this version of the manuscript are specified in the publishing policy. For all terms of use and more information see the publisher's website.

This item was downloaded from IRIS Università di Bologna (https://cris.unibo.it/).
When citing, please refer to the published version.

(Article begins on next page)

09 November 2026

This is the final peer-reviewed accepted manuscript of:

S. Canola, G. Bagnara, Y. Dai, G. Ricci, A. Calzolari, F. Negri, "Addressing the Frenkel and charge transfer character of exciton states with a model Hamiltonian based on dimer calculations: Application to large aggregates of perylene bisimide", J. Chem. Phys. **154**, 124101 (2021).

The final published version is available online at:

https://doi.org/10.1063/5.0045913

Rights / License:

The terms and conditions for the reuse of this version of the manuscript are specified in the publishing policy. For all terms of use and more information see the publisher's website.

Addressing the Frenkel and charge transfer character of exciton states with a model Hamiltonian based on dimer calculations: application to large aggregates of perylene bisimide

*Sofia Canola[a,b], Giuseppe Bagnara[a], Yasi Dai[a], Gaetano Ricci[a,c], Alessandro Calzolari[a] and Fabrizia Negri[a,d]**

[a]Università di Bologna, Dipartimento di Chimica 'Giacomo Ciamician', Via F. Selmi, 2, 40126 Bologna, Italy

[b]Present address: Institute of Physics of the Czech Academy of Sciences, Cukrovarnická 10/112, CZ16200 Praha 6, Czech Republic

[c]Present address: Unité de Chimie Physique Théorique et Structurale & Laboratoire de Physique du Solide, Namur Institute of Structured Matter, Université de Namur, B-5000, Namur, Belgium

[d]INSTM, UdR Bologna, Via F. Selmi, 2, 40126, Bologna, Italy.

*Corresponding author: fabrizia.negri@unibo.it

KEYWORDS Molecular aggregates, Frenkel excitons, Charge transfer excitons, Diabatization, model Hamiltonian, Perylene bisimide, J-aggregate, H-aggregate.

ABSTRACT To understand the influence of interchromophoric arrangements on photo-induced processes and optical properties of aggregates it is fundamental to assess the contribution of local excitations (charge transfer (CT) and Frenkel (FE)), to exciton states. Here we apply a general procedure to analyze the adiabatic exciton states derived from time-dependent density functional theory calculations, in terms of diabatic states chosen to coincide with local excitations within a restricted orbital space. In parallel, motivated by the need of cost-effective approaches to afford the study of larger aggregates, we propose to build a model Hamiltonian based on calculations carried out on dimers composing the aggregate. Both approaches are applied to study excitation energy profiles and CT character modulation induced by interchromophore rearrangements in perylene bisimide aggregates up to a tetramer. The dimer-based approach closely reproduces the results of full-aggregate calculations and an analysis in terms of symmetry-adapted diabatic states discloses the effects of CT/FE interactions on the interchange of the H-/J- character for small longitudinal shifts of the chromophores.

1.Introduction.

Improvements in material design and fabrication has determined tremendous advances and applications in the field of organic optoelectronic materials. [1–3] Intermolecular interactions, which strongly depend on the packing arrangement, play a key role in determining the photo-induced processes in aggregates of organic chromophores and the control of chromophore's assembly has become a challenging target in supramolecular chemistry. [4–14] A parallel effort in conceptual comprehension of the underlying fundamental physics of photoinduced processes has led to deep advancements in understanding the influence of interchromophoric arrangements on the optical properties of aggregates, [15–17] and in modeling the photo-induced relaxation processes leading to excimer formation. [18–20]

The photophysical properties of aggregates are strongly dependent on the nature of exciton states, which can be classified as dominated by Frenkel (FE), charge transfer (CT) character or mixed CT/FE. The role of CT states on photo-induced processes is well established: CT states have been identified as possible mediators in singlet fission [21–27] and have a crucial role in exciton-dissociation, charge-separation and charge-recombination processes in organic photovoltaics. [28,29]

Determining the CT/FE character of exciton states predicted from calculations is therefore an essential task, but because wavefunctions (*wf*) are generally expressed as linear combinations of delocalized excitations (*DEs*), a suitable protocol for character analysis is required and several approaches have been proposed, to expand adiabatic states in terms of diabatic bases. [30–35] [36–43] For molecular aggregates, a natural choice is using localized excitations (*LEs*) as diabatic states, that is FE (or neutral) [44] and CT electron excitations between molecular orbitals (MOs) localized on monomers, [33,37,38,40,41,45] since these provide a physically intuitive framework to understand photo-induced processes.

Electronic couplings between diabatic states can be differentiated according to the nature of the interacting sates. Beside FE/FE Coulomb long-range interactions, the FE/CT interactions can become competitive at short inter-chromophore distance where the molecular orbital overlap is significant and can overcome the FE/FE interactions thereby changing the overall photophysical properties of the aggregate and leading to unconventional or CT mediated J-aggregation. [16,17,46] Vibronic fine structure responds to the magnitude and especially the sign of the Coulomb coupling and several studies have addressed the role of exciton-vibrational couplings to model aggregate's absorption spectra. [16,17,46–50] A large number of computational investigations have focused on dimers of π-conjugated chromophores, [33,51–55] and comparably fewer have discussed aggregates of larger dimension [39,41,56,57] while

calculations for larger stacks are of interest because in most situations excitons are delocalized over a relevant number of monomers. [58]

Perylene bisimide (PBI), a molecule that finds applications in high-performance color pigments and as n-type organic semiconductors in transistors and solar cells, has become an ideal model system [33,41,45,53–55] especially for the potential application of J-aggregates. Previous studies on dimers of PBI [33,41,45,53,54] have thoroughly compared the performance of different quantum-chemical (QC) approaches encompassing configuration interaction truncated to single excitations (CIS), time-dependent density functional theory (TD-DFT), and highly accurate levels of theory as spin-component-scaling (SCS) coupled cluster to second order (CC2) [59,60] and SCS algebraic diagrammatic construction to the second-order (ADC(2)) [61]. In most of these studies, the application of a diabatization procedure to exciton adiabatic states, provided insight on the character of each selected eigenstate and therefore on aggregate photo-physics.

Studying the effect of interchromophore displacements or rearrangements on exciton states of large aggregates may put severe limitations to the level of theory that can be afforded. As an alternative to full-aggregate QC calculations, exciton models with different flavors of parametrization protocols have been proposed. [32,62–68] Motivated by the need of cost-effective approaches providing results of quality comparable to full-aggregate calculations, and inspired by previous pioneering work in which the dimer approach was introduced [57] or used to parametrize exciton Hamiltonians [65] here we propose and test a model Hamiltonian (***mH***) built on the basis of QC calculations carried out only on the dimers composing the aggregate. We use the ***mH*** to determine excitation energies and character of the exciton states of trimers and tetramers of PBI for interchromophore displacements along the longitudinal translation coordinate. The QC approach selected is TD-DFT, being a cost-effective method that can be used to compare the results of the cheaper ***mH*** approach with those of full-aggregate

calculations that are also reported here for all the aggregates investigated. This study is therefore developed as follows: first, a diabatization procedure is introduced and applied to full-aggregate calculations on dimers, trimers and tetramers of PBI, to derive a matrix representation of the Hamiltonian, $\boldsymbol{H_{dia}}$ in the diabatic basis formed by LEs within the selected orbital space. Second, the $\boldsymbol{mH}$ is built for trimer and tetramer, on the basis of dimer calculations and the results (adiabatic energy profiles, CT/FE character of exciton states, magnitude of $\boldsymbol{mH}$ matrix elements) are compared with those obtained from full-aggregate calculations, to assess the quality of the less expensive approach. Furthermore, to unravel the effects of CT/FE interactions leading to J-aggregation for short longitudinal shifts, the use of symmetry-adapted diabatic bases is applied to dimers and trimers of PBI.

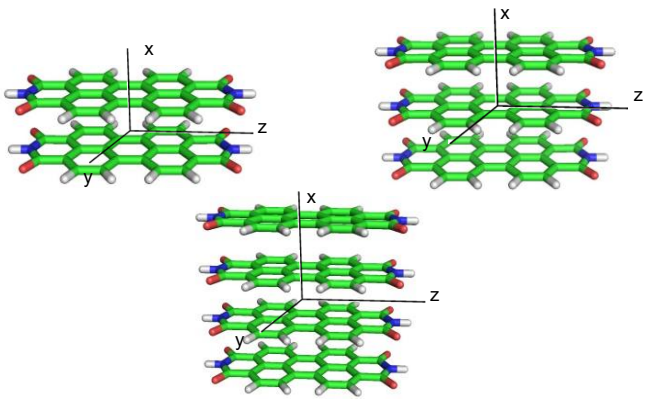

Figure 1. The PBI aggregates considered in this work. Exciton states have been determined at the eclipsed configuration shown here and along the interchromophore longitudinal (z) translation coordinate.

2. Theoretical background.

2.1. Character analysis of exciton states via diabatization.

Before discussing the details of the protocol used to analyze exciton state character, we introduce the choices made as regard a) diabatic basis, b) orbital space and c) dimension of the adiabatic state space.

The adiabatic exciton states obtained from most QC calculations are generally expressed as linear combinations of *DEs* built from delocalized molecular orbitals (DMOs). To analyze the exciton *wf* character it is more convenient to express the adiabatic states on a basis of *LE*s, in turn built on a basis of monomer localized molecular orbitals (LMOs). The *LE*s can be further distinguished in neutral excitations localized on a single monomer and CT excitations involving two of the ***n*** molecules forming the aggregate. We will label for simplicity the neutral localized excitations as FE [44] since their linear combinations form the FE excitons.

A diabatic representation is a convenient tool to characterize the nature of the electronic states. Several approaches have been discussed to determine a diabatic basis by variously defined transformations of previously computed adiabatic states or by determining a set of wavefunctions that are weakly dependent on nuclear coordinates. [33–41] A natural choice for the definition of a diabatic representation, used in this work as in several previous investigations [37,38,40,41,45], is represented by the set of *LEs*.

One relevant condition, when undergoing the character analysis of exciton states obtained from QC calculations, concerns the dimension of the adiabatic/diabatic basis of states included in the analysis, which depends on the dimension of the selected active orbital space (AOS) from which electron excitations are generated. A common assumption is the minimal orbital space (MIOS), with two electrons in two orbitals, usually the HOMO and LUMO of each monomer forming the aggregate. [37,40,44,45,69] This choice restricts the application to molecules whose lowest excited state is dipole allowed and well described by the HOMO→LUMO excitation, such as PBI. Although the analysis of the aggregate excited states in this work is

always carried out in the framework of the MIOS, the AOS could be straightforwardly expanded, including additional orbitals of each monomer. [35,52]

In the framework of TD-DFT calculations, the exciton *wf* is described by single excitations. Restricting the attention to the MIOS, the number of single excitations, for an aggregate of $\boldsymbol{n}$ molecules, is $\boldsymbol{n^2}$, implying that only the computed adiabatic exciton states whose *wf* is dominated by some of the $\boldsymbol{n^2}$ excitations, are considered for character analysis and diabatization. Accordingly, $\boldsymbol{n^2}$ is the dimension of the Hamiltonian's matrix representation in the adiabatic $\boldsymbol{H}_{adia}$ and in the diabatic $\boldsymbol{H}_{dia}$ state basis. The diabatic *LE* basis of the aggregate encompasses $\boldsymbol{n}$ FE states, localized on each molecular unit, and $\boldsymbol{n^2 - n}$ CT states involving two different monomers.

Having introduced the choices made in this work as regard the diabatic basis, orbital and adiabatic state spaces, we present in the following the protocol for character state analysis. Each subsection corresponds to the sequential items of the workflow shown in Figure 2.

DMOs as linear combinations of LMOs. In the first step of the character analysis, the DMOs are expressed as linear combinations of the LMOs by the application of a projection operator, following the procedure outlined in previous work: [70,71]

$$|\psi_{MON_i}\rangle\langle\psi_{MON_i}|\psi_{AGGR_j}\rangle = C_{i,j}^{AGGR_MOB}|\psi_{MON_i}\rangle \quad (1)$$

Where $|\psi_{MON_i}\rangle$ are the molecular orbitals of the isolated monomers in the atomic orbital basis (AOB) and $|\psi_{AGGR_j}\rangle$ are the aggregate molecular orbitals in the AOB. In matrix formulation $|\psi_{MON_i}\rangle$ form the column vectors of the $\boldsymbol{C}_{MON_AOB}$ matrix which is therefore a block diagonal matrix containing the MOs coefficients in the AOB from each monomer, with off block diagonals set to zero. Similarly, $|\psi_{AGGR_j}\rangle$ form the column vectors of the $\boldsymbol{C}_{AGGR_AOB}$ matrix.

The linear combinations describing DMOs in terms of LMOs are defined by the $C_{i,j}^{AGGR_MOB}$ coefficients in the monomer orbital basis (MOB) which, for a given aggregate orbital *j*, form the columns of the $\boldsymbol{C}_{AGGR_MOB}$ matrix and are obtained as:

$$\boldsymbol{C}_{AGGR_MOB} = \boldsymbol{C}_{MON_AOB}^{\boldsymbol{t}} \cdot \boldsymbol{S}_{MON_AOB} \cdot \boldsymbol{C}_{AGGR_AOB} \tag{2}$$

where the $\boldsymbol{S}_{MON_AOB}$ is the overlap matrix of the monomers in the AOB and the superscript $\boldsymbol{t}$ indicates the transpose.

The overlap matrix in the MOB is then required to orthogonalize, using Löwdin's symmetric transformation, [72] the monomer orbitals belonging to different monomers. The overlap matrix $\boldsymbol{S}_{AGGR_MOB}$ between the LMOs is calculated from the MO coefficients of the monomer orbitals and the overlap of the atomic orbitals in the aggregate configuration $\boldsymbol{S}_{AGGR_AOB}$.

$$\boldsymbol{S}_{AGGR_MOB} = \boldsymbol{C}_{MON_AOB}^{\boldsymbol{t}} \cdot \boldsymbol{S}_{AGGR_AOB} \cdot \boldsymbol{C}_{MON_AOB} \tag{3}$$

Finally, the aggregate's orbitals expressed in terms of orthogonalized monomer orbitals form the columns of the $\boldsymbol{C}_{AGGR_MOB}^{L}$ matrix (superscript *L* indicates that Löwdin's orthogonalization has been applied) and are obtained as [70,71]

$$\boldsymbol{C}_{AGGR_MOB}^{L} = \boldsymbol{S}_{AGGR_MOB}^{-\frac{\mathbf{1}}{\mathbf{2}}} \cdot \boldsymbol{C}_{AGGR_MOB} \tag{4}$$

The dimension of the $\boldsymbol{C}_{AGGR_MOB}^{L}$ matrix corresponds to the full dimension of the MOB, however, the occupied DMOs belonging to the MIOS are mainly determined by the occupied LMOs belonging to the MIOS and similarly for the unoccupied MOs. Therefore, only the submatrices $\boldsymbol{MIOS_O}_{AGGR_MOB}^{L}$ (for occupied MOs) and $\boldsymbol{MIOS_U}_{AGGR_MOB}^{L}$ (for unoccupied MOs) extracted from $\boldsymbol{C}_{AGGR_MOB}^{L}$ are retained, Löwdin orthogonalized, and used in the subsequent steps.

DEs as linear combinations of LEs within the MIOS. With the DMOs expressed as linear combinations of LMOs belonging to the MIOS, a generic *DE* ($i \rightarrow j$) from an occupied *i* to an

empty *j* DMO can be expanded in terms of *LEs* $(k \rightarrow l)$ between LMOs. The coefficients of such expansion are given by

$$U_{k\rightarrow l,i\rightarrow j}^{DE\rightarrow LE} = MIOS_O_{k,i}^{AGGR_MOB,L} \cdot MIOS_U_{l,j}^{AGGR_MOB,L} \quad (5)$$

where $MIOS_O_{k,i}^{AGGR_MOB,L}$ and $MIOS_U_{l,j}^{AGGR_MOB,L}$ are orthogonalized expansion coefficients of aggregate's occupied and empty orbitals, respectively, in the MOB. The elements computed by Eq. (5) form the unitary matrix $\boldsymbol{U_{DE\rightarrow LE}}$ whose columns describe each *DE* $(i \rightarrow j)$ excitation in terms of the *LEs* $(k \rightarrow l)$ excitations.

QC exciton state calculations and adiabatic states selection. From QC calculations on the aggregate, the subset of $\boldsymbol{n^2}$ exciton states originated from the MIOS (expressed in terms of *DEs*), are selected out of the full set of computed eigenstates, Gram-Schmidt orthogonalized [73] and used to form the columns of the $\boldsymbol{C_{DE}^{adia}}$ matrix. The corresponding $\boldsymbol{n^2}$ eigenvalues (excitation energies) form the diagonal $\boldsymbol{H_{adia}}$ matrix.

Adiabatic states as linear combinations of LEs. The CT/FE nature of each adiabatic exciton state is readily obtained by its expansion in terms of *LE*s, $\boldsymbol{C_{LE}^{adia}}$, via the following matrix multiplication:

$$\boldsymbol{C_{LE}^{adia}} = \boldsymbol{U_{DE\rightarrow LE}} \cdot \boldsymbol{C_{DE}^{adia}} \quad (6)$$

Hamiltonian in the diabatic basis. Furthermore, the diabatization scheme in the framework of the selected AOS**,** in line with others available in literature, [36,38,40,74] allows to obtain a matrix representation of the Hamiltonian in the diabatic *LE* basis, $\boldsymbol{H_{dia}}$, via the following matrix transformation:

$$\boldsymbol{H_{dia}} = \boldsymbol{C_{LE}^{adia}} \cdot \boldsymbol{H_{adia}} \cdot \boldsymbol{C_{LE}^{adia^t}} \quad (7)$$

We have verified that upon diagonalization of $\boldsymbol{H}_{dia}$ exactly the same adiabatic eigenvalues and eigenvectors obtained from the QC calculations are recovered (see also the supplementary material).

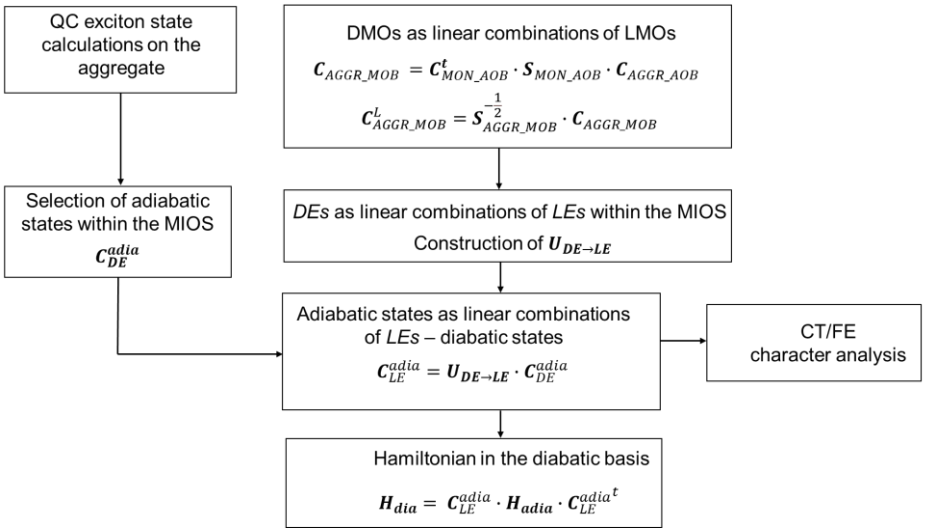

Figure 2. Workflow for exciton state character analysis and diabatization.

For aggregates characterized by the presence of symmetry, the simple *LE* basis may not be the most suitable choice to analyze the CT/FE character of adiabatic exciton states. In these cases a symmetry-adapted combinations of CT (also known as charge resonances [75]) and FE diabatic states are more effective [37,45] and will be used here for the dimer and the trimer of PBI. In the following however, if not otherwise stated, the diabatic basis coincides with the set of *LEs.*

2.2. Construction of a simplified, dimer based, model Hamiltonian *mH*.

The elements of the $\boldsymbol{H}_{dia}$ matrix for a dimer (Eq.(7) and Table S1), have been discussed and analyzed in several previous studies [36,37,45,69]. If we indicate with $\boldsymbol{a}$ and $\boldsymbol{b}$ the two monomers that define a dimer, the four *LEs* forming the diabatic basis in the MIOS are the two FE $\boldsymbol{a}^{*}\boldsymbol{b}$, $\boldsymbol{a}\boldsymbol{b}^{*}$ states and the two CT $\boldsymbol{a}^{+}\boldsymbol{b}^{-}, \boldsymbol{a}^{-}\boldsymbol{b}^{+}$ states. Specifically, the connection between the elements of $\boldsymbol{H}_{dia}$ and the matrix elements of a frontier-orbitals configuration interaction

singles, was derived [45,76] according to Slater–Condon (SC) rules [77]. This connection allowed to rationalize the magnitude of the elements of $\boldsymbol{H}_{dia}$ by considering the integrals that define each matrix element. For molecules equivalent by symmetry, the elements forming the $\boldsymbol{H}_{dia}$ of a dimer are collected in Table S1 where E_{FE}, E_{CT} are the energies of FE and CT diabatic states, V_e is the exciton (or Coulomb dominated) long-range interaction, W is the interaction between CT states and D_e, D_h are the coupling matrix elements for electron transfer (charge transfer integrals) that are widely used to study hole and particle transport. [78–81]

Here we propose to use the TD-DFT derived $\boldsymbol{H}_{dia}$ matrix elements of dimers characterized by different interplanar distances, to build a $\boldsymbol{mH}$ for larger aggregates. For an aggregate formed by three or more molecules, the $\boldsymbol{mH}$ represents an approximation of the $\boldsymbol{H}_{dia}$ obtained from full-aggregate QC calculations discussed in the previous section but it is expected to provide a cheap alternative to analyze energy profiles, character of exciton states and other exciton state properties such as the interchange from H- to J- spectroscopic features.

The elements forming the $\boldsymbol{mH}$ are identified on the basis of the dimers D1, D2, D3, etc. (with different interplanar distances) forming the aggregate of $\boldsymbol{n}$ molecules (see Figure 3). By partitioning the aggregate in terms of the composing dimers, each element of $\boldsymbol{mH}$ can be related to one of the elements of the $\boldsymbol{H}_{dia}$ of the corresponding dimer. The connection can be readily determined by considering that each $\boldsymbol{H}_{dia}$ matrix element of the larger aggregate is an integral whose expression can also be inferred from SC rules [77], with a straightforward generalization of the strategy employed in previous work [45,76] to identify the elements for a dimer.

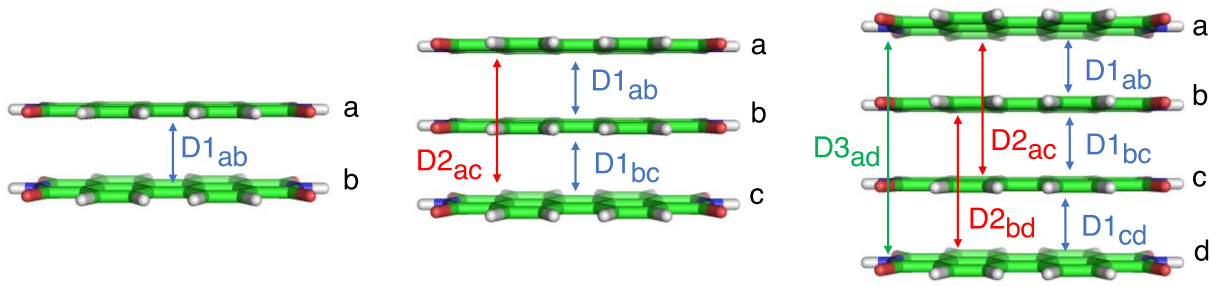

Figure 3. Scheme for the construction of the simplified ***mH*** for dimer, trimer and tetramer.

Thus, to describe the trimer in Figure 3, formed by the three monomers ***a***, ***b***, ***c***, one needs to calculate two types of dimers: D1 with the two monomers at short distance and D2 whose molecules are located at a distance which is twice as big. The diabatic basis is formed by three FE excitations ($\boldsymbol{a^*bc}$, $\boldsymbol{ab^*c}$, $\boldsymbol{abc^*}$) and six CT excitations ($\boldsymbol{a^+b^-c}$, $\boldsymbol{a^-b^+c}$, $\boldsymbol{ab^+c^-}$, $\boldsymbol{ab^-c^+}$, $\boldsymbol{a^+bc^-}$, $\boldsymbol{a^-bc^+}$), four of which labelled as CT1 (corresponding to short-distance dimers D1) and the last two labelled as CT2 (corresponding to the large-distance dimer D2). The resulting ***mH*** matrix is shown in Figure 4, whose elements are labelled according to their counterpart taken from the $\boldsymbol{H}_{dia}$ of the composing dimers and the superscript (1) and (2) refer to dimer D1 and D2, respectively. Some of the ***mH*** matrix elements of the trimer (and similarly for larger aggregates) do not correspond to any of the $\boldsymbol{H}_{dia}$ elements of D1 or D2. These elements, according to SC rules, correspond to integrals that contain differential overlaps and are therefore expected to be very small. For this reason, they were approximated to zero in Figure 4.

mH	$\boldsymbol{a^*bc}$	$\boldsymbol{ab^*c}$	$\boldsymbol{abc^*}$	$\boldsymbol{a^+b^-c}$	$\boldsymbol{a^-b^+c}$	$\boldsymbol{ab^+c^-}$	$\boldsymbol{ab^-c^+}$	$\boldsymbol{a^+bc^-}$	$\boldsymbol{a^-bc^+}$
$\boldsymbol{a^*bc}$	E_{FE}	$Ve^{(1)}$	$Ve^{(2)}$	$D_e^{(1)}$	$D_h^{(1)}$	0	0	$D_e^{(2)}$	$D_h^{(2)}$
$\boldsymbol{ab^*c}$	$Ve^{(1)}$	E_{FE}	$Ve^{(1)}$	$D_h^{(1)}$	$D_e^{(1)}$	$D_e^{(1)}$	$D_h^{(1)}$	0	0
$\boldsymbol{abc^*}$	$Ve^{(2)}$	$Ve^{(1)}$	E_{FE}	0	0	$D_h^{(1)}$	$D_e^{(1)}$	$D_h^{(2)}$	$D_e^{(2)}$
$\boldsymbol{a^+b^-c}$	$D_e^{(1)}$	$D_h^{(1)}$	0	$E_{CT}^{(1)}$	$W^{(1)}$	0	$D_h^{(2)}$	$D_e^{(1)}$	0
$\boldsymbol{a^-b^+c}$	$D_h^{(1)}$	$D_e^{(1)}$	0	$W^{(1)}$	$E_{CT}^{(1)}$	$D_e^{(2)}$	0	0	$D_h^{(1)}$
$\boldsymbol{ab^+c^-}$	0	$D_e^{(1)}$	$D_h^{(1)}$	0	$D_e^{(2)}$	$E_{CT}^{(1)}$	$W^{(1)}$	$D_h^{(1)}$	0
$\boldsymbol{ab^-c^+}$	0	$D_h^{(1)}$	$D_e^{(1)}$	$D_h^{(2)}$	0	$W^{(1)}$	$E_{CT}^{(1)}$	0	$D_e^{(1)}$
$\boldsymbol{a^+bc^-}$	$D_e^{(2)}$	0	$D_h^{(2)}$	$D_e^{(1)}$	0	$D_h^{(1)}$	0	$E_{CT}^{(2)}$	$W^{(2)}$
$\boldsymbol{a^-bc^+}$	$D_h^{(2)}$	0	$D_e^{(2)}$	0	$D_h^{(1)}$	0	$D_e^{(1)}$	$W^{(2)}$	$E_{CT}^{(2)}$

Figure 4: matrix elements of ***mH*** for a trimer. The color code refers to the two different types of dimers D1 and D2 (see Figure 3) used to decompose the trimer aggregate and to establish

the connection between matrix elements of the trimer and those of the $\boldsymbol{H}_{dia}$ of the composing dimers.

2.3. Computational details.

The PBI monomer structure was the same used in previous investigations on PBI aggregates, optimized at the BLYP-D/TZV(P) level of theory. [82] The distance between the planes of different monomers was set to 3.4 Å which is a distance used in previous investigations on dimers of PBI. The exciton states were computed for the eclipsed aggregates and for displacements of 0.5 Å up to 8.0 Å, along the longitudinal translation coordinate (z) (see Figure 1 and Figure S1). Because the calculations on dimers D2, D3 were used to build the ***mH*** of trimers and tetramers, note that the longitudinal shifts of sequential configurations were twice as big for dimer D2 (i.e. shifts of 1.0 Å up to 16.0 Å) and three times as big for dimers D3 (i.e. shifts of 1.5 Å up to 24.0 Å) (See Figure S1).

Excitation energies were determined with TD-DFT calculations using the ωB97XD functional and the 6-31G* basis set. The ωB97XD functional was chosen owing to its reliable description of charge transfer states as reported in previous investigations of the PBI dimer. [33] All QC calculations were carried out with the Gaussian16 suite of programs. [83]

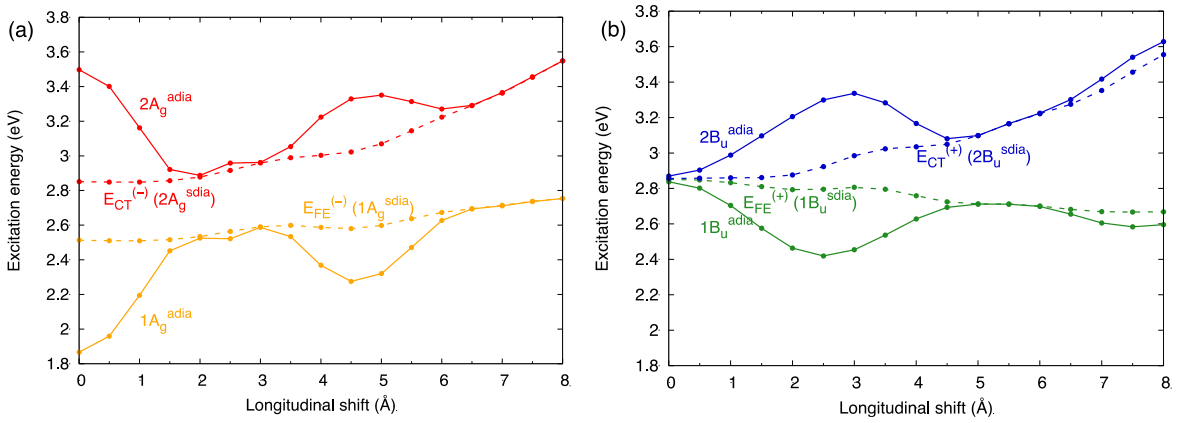

Figure 5. Energy profiles of symmetry-adapted diabatic (*sdia*, dashed) states and adiabatic (*adia*, solid) states for the dimer of PBI at 3.4 Å. The *adia* states result from the CT/FE interactions (shown in Figure 6a) between *sdia* states of the same symmetry. When the interactions are large, the *adia* states are pushed far apart one another. (a) A_g states and (b) B_u states of the dimer at distance 3.4 Å, from TD-ωB97XD/6-31G* calculations.

3. Results.

3.1. PBI dimers.

Previous investigations of excitation energy profiles and CT/FE character of PBI dimers, for inter-chromophoric longitudinal shifts, have shown that QC computed exciton states are generally strong mixtures of the two types of *LEs* and the weight of FE and CT characters critically depends on the energy difference between diabatic states and their coupling. [33,45] The adiabatic energy profiles and CT character of the four exciton states (see Figure S2) from the TD-ωB97XD/6-31G* calculations reported here are in line with the above discussed results. Interestingly the CT character of the lowest state of B_u (and A_g) symmetry is lower than 50% for all geometries along the longitudinal translation coordinate, in agreement with the results of high-level QC calculations. [33,45] The weight of the CT character can be traced back to the energy location of symmetry-adapted diabatic (*sdia*) states, (a more suitable diabatic basis in this case, due to the high symmetry of the aggregate) defined by the combinations in Table S2. More specifically, the amount of CT character (always $< 50\%$ for the lowest B_u and A_g states) is determined by the energy location of the ${E_{FE}}^{(\pm)}$ *sdia* state, always below the ${E_{CT}}^{(\pm)}$ state in the calculations presented here, in agreement with the results of reference high-level calculations and in contrast with the results of other long-range corrected functionals or CIS. [33,45]

The oscillating trend in adiabatic energy profiles (Figure 5) and the corresponding CT character (Figure S2), are readily rationalized by the oscillating trend of the interactions between CT and FE *sdia* states. As shown in Table S3, these interactions are proportional to the + and – combinations (collected in Figure 6a) of the D_e and D_h elements, whose dependence on the longitudinal translation is also oscillating (Figure S3). The CT/FE interaction competes with the exciton coupling in determining the photophysical properties of the aggregate. This is the well-known mechanism of CT mediated J-aggregation, [16,17,46] leading to the appearance of J-type spectroscopic features for small longitudinal displacements. This unconventional behavior, not understood within Kasha's theory, has been rationalized by the presence of CT states creating an effective short-range exciton coupling that can induce J-type spectroscopic features. [16,17,45,46,53,71,84,85] The oscillation of the CT/FE interaction between *sdia* states of B_u symmetry along the longitudinal shift, proportional to the $D_e + D_h$ profile shown in Figure 6a, determines an interchange of the lowest exciton states of A_g and B_u symmetry in the dimer, for longitudinal shifts in the range of 2-3 Å (see Figure S2a), where $D_e + D_h$ shows a maximum (see Figure 6a). This interaction pushes the adiabatic $1B_u$ state below the $1A_g$ state (see Figure 5b and Figure S2a) and leads to the well-known switch from H- to J-aggregate for the dimer. [16]

Beside the dimer with monomers at 3.4 Å distance, also dimers with interplanar distances of 6.8 Å and 10.2 Å were investigated, since the corresponding $\boldsymbol{H_{dia}}$ matrix elements were used to build the $\boldsymbol{mH}$ for larger aggregates. For such large interplanar distances, the interactions between diabatic states are drastically reduced. This, together with the increased energy of CT diabatic states (see the CT1, CT2 and CT3 energy profiles in Figure 6b), leads to adiabatic states that keep an almost complete FE or CT character and they are not further discussed here.

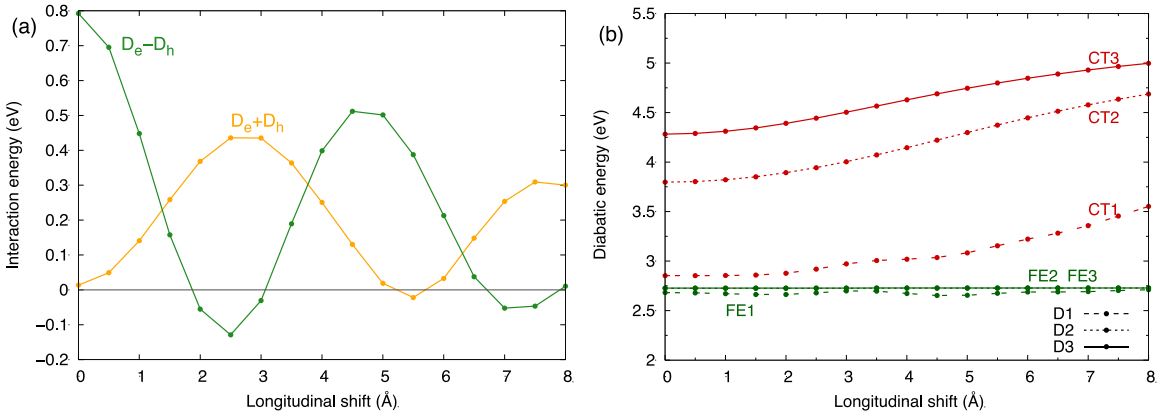

Figure 6. (a) Magnitude and modulation along the longitudinal translation coordinate, of the $D_e \pm D_h$ terms, proportional to the interaction between CT/FE symmetry-adapted diabatic states of the dimer and trimer (see also Tables S3, S5); (b) Comparison between diabatic energy profiles of FE and CT states for the dimer of PBI at distances 3.4 Å (dimer D1 in Figure 3, diabatic energies: FE1 and CT1), 6.8 Å (dimer D2 in Figure 3, diabatic energies: FE2 and CT2) and 10.2 Å (dimer D3 in Figure 3, diabatic energies: FE3 and CT3). From TD-ωB97XD/6-31G* calculations.

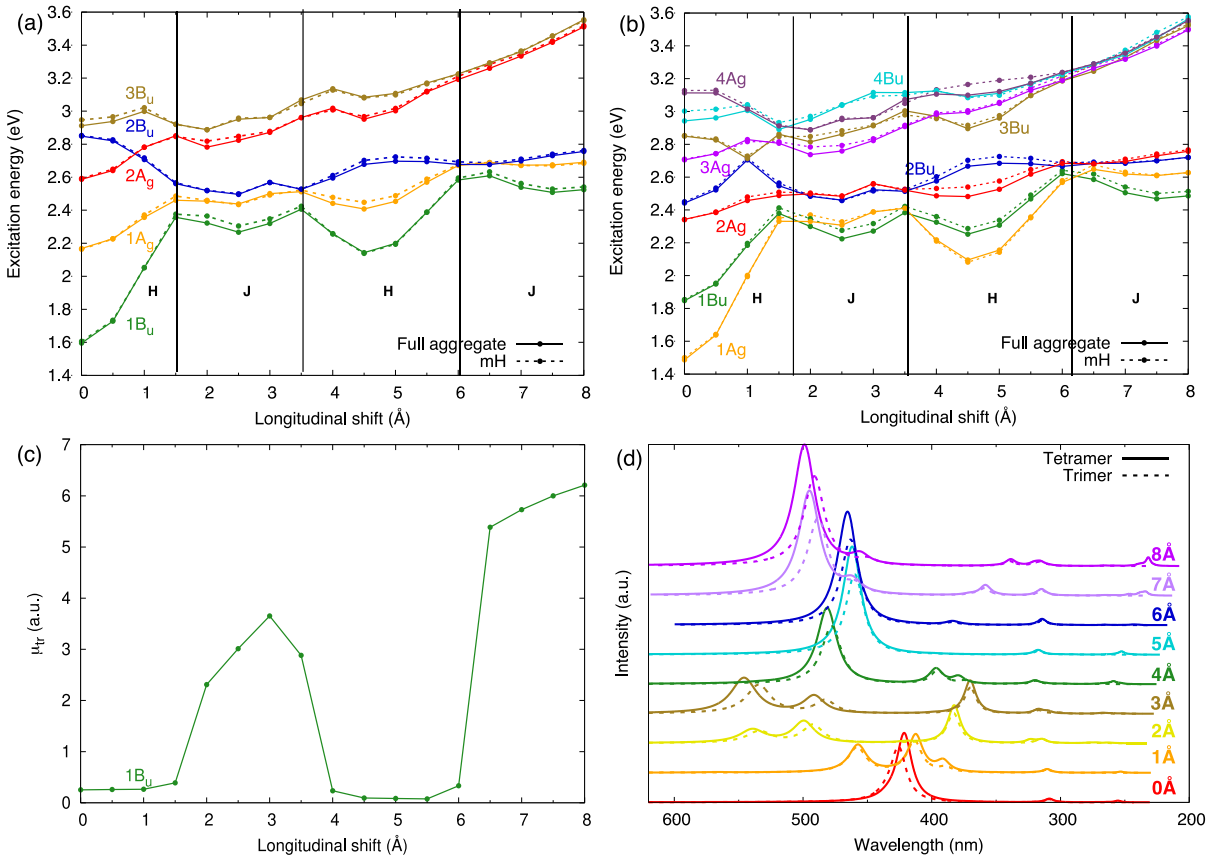

Figure 7. Low lying exciton states of (a) the PBI trimer and (b) the tetramer from full-aggregate calculations (solid) and from diagonalization of the ***mH*** built from dimer calculations (dashed). (c) Transition dipole moment of the lowest energy exciton state of the trimer, from TD-ωB97XD/6-31G* calculations. (d) Comparison between vertical absorption spectra predicted for the trimer (dashed) and the tetramer (solid). Intensity modulation induced by the longitudinal shift from 0 Å to 8 Å. Different colours are used to distinguish the spectra computed for different displacements.

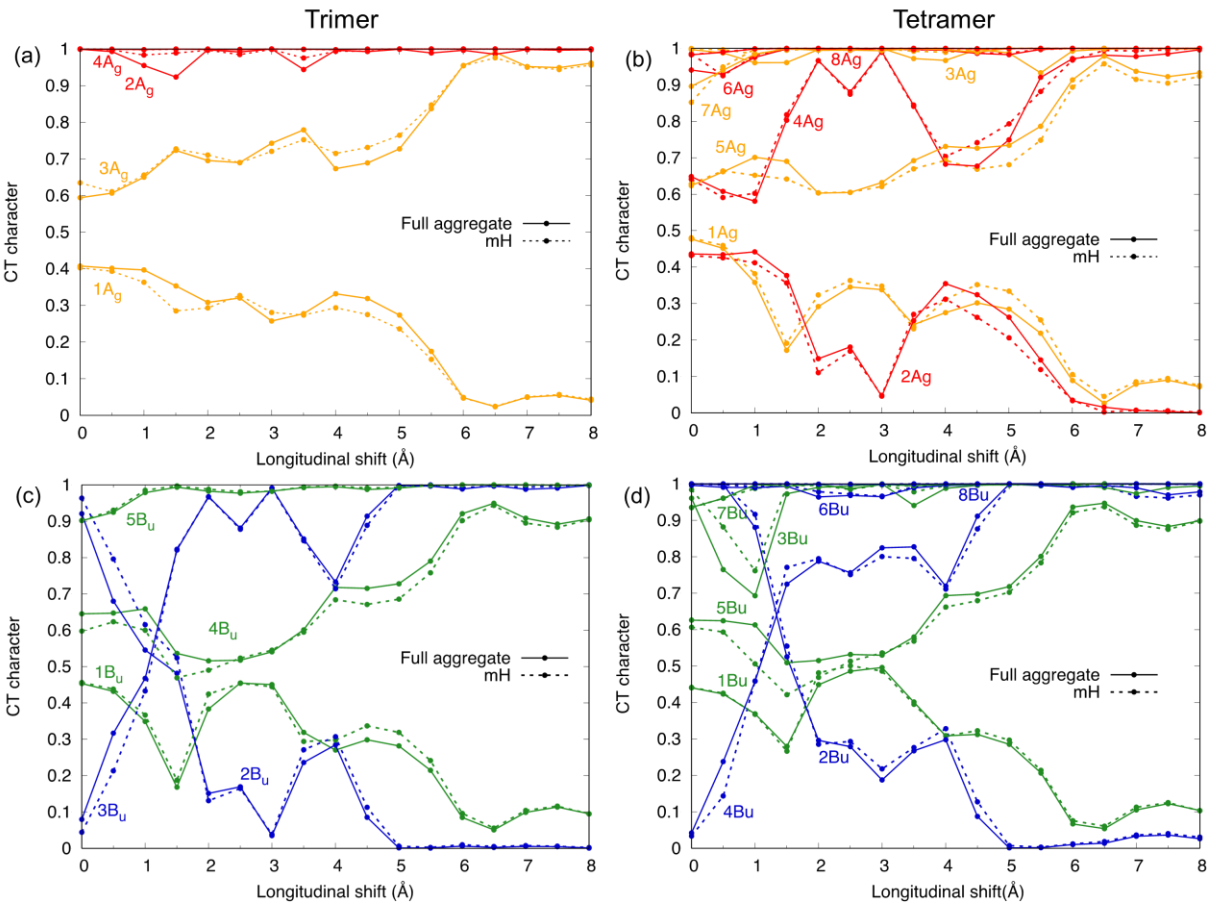

Figure 8. Modulation of the CT character of the 9 exciton states (5 of B_u and 4 of A_g symmetry) of the PBI trimer and of the 16 exciton states (8 of B_u and 8 of A_g symmetry) of the PBI tetramer, as a function of the longitudinal displacement. The A_g exciton states of the trimer are shown in panel (a), those of the tetramer in panel (b). The B_u exciton states of the trimer are shown in panel (c), those of the tetramer in panel (d). In each panel the CT character of the adiabatic states determined from TD-ωB97XD/6-31G* calculations on the full-aggregate (solid) and those resulting from diagonalization of the ***mH*** (dotted) are compared.

3.2. PBI trimer and tetramer

For the PBI trimer and tetramer, two sets of results are compared: 1) exciton states determined with TD-ωB97XD/6-31G* calculations carried out on the full aggregate, whose adiabatic states originated from the MIOS were subject to the diabatization procedure described

in section 2.1 to obtain the $\boldsymbol{H_{dia}}$ matrix and the CT/FE character of each state; 2) exciton states and CT/FE character determined from diagonalization of the $\boldsymbol{mH}$ matrix, built on the basis of TD-ωB97XD/6-31G* calculations carried out on the dimers composing the aggregate as discussed in sections 2.2, 2.3. The excitation energy profiles of the adiabatic states, obtained from the two approaches (see Figure 7a,b and Figure S4) are very similar, an indication that the $\boldsymbol{mH}$ approach reproduces well the excitation energies of full-aggregate calculations. We note that, compared to the dimer, the lowest energy exciton state of the trimer is always $1B_u$ and therefore implies a symmetry allowed transition for all longitudinal shifts. However, the computed transition dipole moment of the $1B_u$ state of the trimer (see Figure 7c and Figure S5 for the transition dipole moments of higher energy B_u states) switches from very low values typical of an H-aggregate (in the interval 0.0 Å - 1.5 Å and 6.5 Å - 8.0 Å) to larger values typical of J-aggregates (in the interval 2.0 Å -3.5 Å and 4.0 Å to 6.0 Å) thereby determining an interchange of H- and J- spectroscopic features very similar to the well-established predictions for a PBI dimer. [16,17,45,46,53,71,84,85] For the tetramer the situation is much closer to the dimer, since the lowest energy exciton state (Figure 7b) switches from A_g to B_u and drives an interchange of H-/J-/H-/J-aggregate character as in the dimer. In summary, both trimer and tetramer display the typical switch to J-aggregation for small longitudinal shifts followed by further H-/J- interchanges and, accordingly, they display a very similar modulation of computed vertical absorption spectra along the longitudinal translation (see Figure 7d).

Figure 8 compares the CT character determined by the two approaches, for the nine (five of B_u and four of A_g symmetry) and sixteen (eight of B_u and eight of A_g symmetry) adiabatic states resulting by excitations within the MIOS for the trimer and tetramer, respectively. The differences are slightly more significant compared to those observed in the energy profiles, but do not affect substantially the character of a given exciton state, whose dominant CT or FE character remains the same for both approaches. The similar character description is clearly

seen in Figure 9 for the eclipsed 0.0 Å configuration of both aggregates, and in Figures S6 for additional geometric configurations taken along the longitudinal translation. The profiles of the $\boldsymbol{H_{dia}}$ and $\boldsymbol{mH}$ diagonal and off-diagonal matrix elements of the trimer, collected in Figure 10 and Figure S7, allow to critically assess the more approximate $\boldsymbol{mH}$. The first difference between the $\boldsymbol{H_{dia}}$ and $\boldsymbol{mH}$ concerns the diabatic energy profiles of the three $\boldsymbol{E_{FE}}$ terms that, for $\boldsymbol{mH}$, are chosen to be identical to those computed for the dimer D1, according to the definition in Figure 4. In contrast, two slightly different energy profiles are extracted from $\boldsymbol{H_{dia}}$, one corresponding to the energy of the FE diabatic states centered on monomer $\boldsymbol{b}$, labelled FE_b and the second corresponding to the two degenerate FE diabatic states centered on the terminal monomers $\boldsymbol{a}$ and $\boldsymbol{c}$ (FE_a and FE_c). While the latter are very similar to the $\boldsymbol{E_{FE}}$ extracted from D1 calculations, the former is slightly lower, as a result of the different chemical environment of terminal and central monomers, a distinction which is missing in building the $\boldsymbol{mH}$. Similarly, only one energy profile for CT diabatic states involving monomers 3.4 Å apart (CT1) or 6.4 Å apart (CT2) is used to build $\boldsymbol{mH}$, (see Figure 4) while two slightly different energy profiles for CT1 diabatic states are extracted from the $\boldsymbol{H_{dia}}$ matrix determined by diabatization of full-aggregate calculations. It should be noted that the additional differences between the CT energy profiles obtained from $\boldsymbol{H_{dia}}$ and $\boldsymbol{mH}$ in the regions 1-2 Å and 4-5 Å are likely to be due to the additional number of adiabatic states generated by full-aggregate TD-DFT calculations, beyond those selected within the MIOS. Concerning off-diagonal matrix elements, in Figure 10b we compare the $V_e^{(1)}$ and $V_e^{(2)}$ interactions extracted from the $\boldsymbol{mH}$ matrices (see Figure 4) with the corresponding elements in the $\boldsymbol{H_{dia}}$ matrices, while in Figure S7 we collect the comparison for $D_e^{(1,2)}/D_h^{(1,2)}$ elements. The differences between full-aggregate calculations and the dimer approach are acceptably small for both $V_e^{(1,2)}$ and $D_e^{(1,2)}/D_h^{(1,2)}$ elements. The largest discrepancy is determined for the matrix elements identified as $D_e^{(2)}/D_h^{(2)}$ in $\boldsymbol{mH}$ (Figure 4) which are underestimated compared to the corresponding elements extracted from $\boldsymbol{H_{dia}}$.

Interestingly, for this aggregate the presence of the molecule in between the two distant monomers (in full-aggregate calculations) does not screen these interaction terms, which are larger than those introduced in building the ***mH,*** possibly as a result of indirect interactions mediated by the central molecule which is missing in the ***mH*** approach.

These differences, in all cases, are not large but, together with other similar approximations in the off-diagonal elements of ***mH***, account for the small discrepancies above discussed, some of which could be corrected by building the elements of ***mH*** from non-symmetric dimer calculations or taking advantage of solvent effects [56,86] to simulate the embedding of internal monomers.

Finally, we note that interactions ($V_e^{(2)}$) between FE diabatic states that are not near-neighbors are not negligible, which suggests that for the aggregates investigated in this work it would not be appropriate to approximate the interaction terms only to near neighbors.

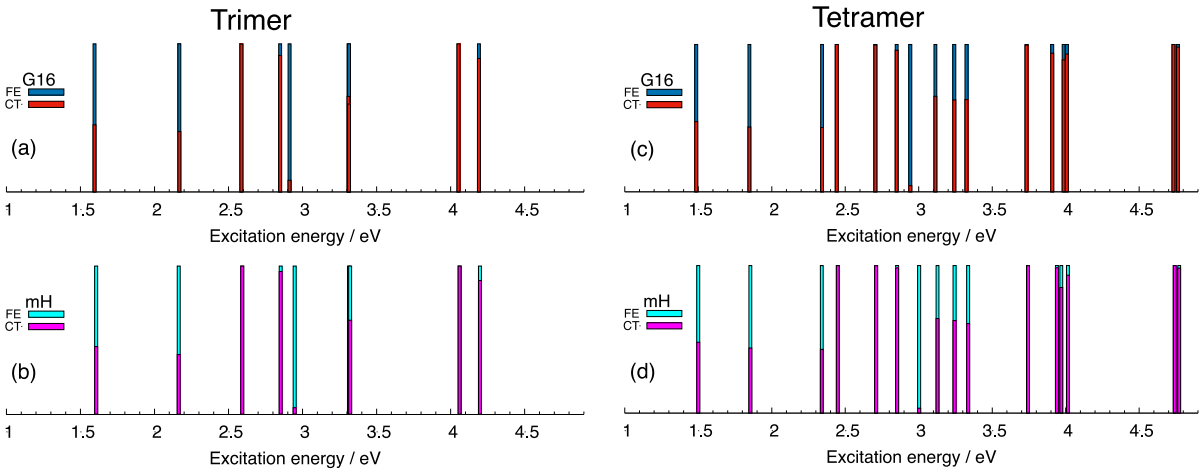

Figure 9. The CT/FE character of exciton states: results for (left) PBI trimer and (right) PBI tetramer: (a, c) from full-aggregate (G16 label) TD-ωB97XD/6-31G* calculations and (b, d) from ***mH***. The longitudinal displacement is 0.0 Å.

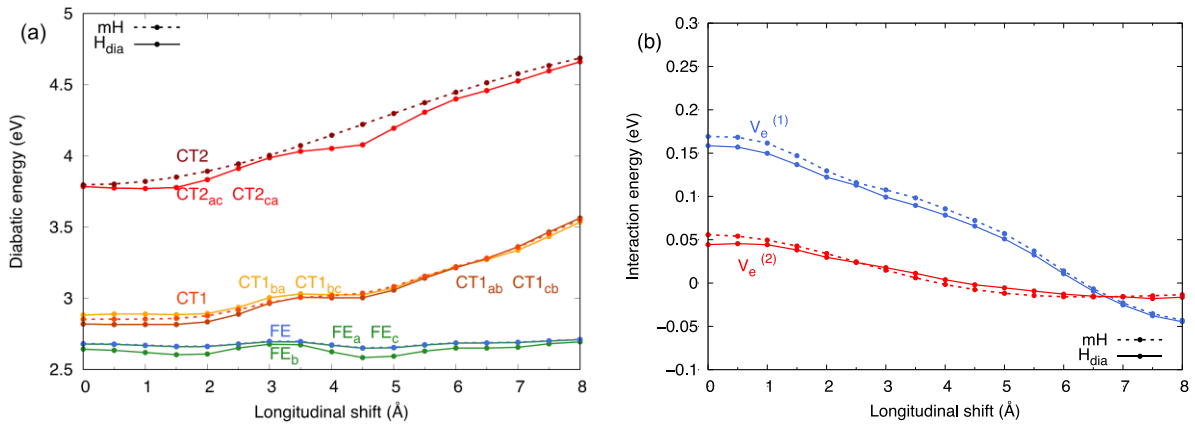

Figure 10. (a) Comparison between FE/CT diabatic state energy profiles for the trimer of PBI from (solid) $\boldsymbol{H_{dia}}$ and (dashed) $\boldsymbol{mH}$. The energies of the three FE (neutral) diabatic states extracted from $\boldsymbol{H_{dia}}$ are not identical and are identified by a subscript letter indicating the monomer to which they correspond. Similarly, the energies of the four CT1 diabatic states extracted from $\boldsymbol{H_{dia}}$ are not identical and each diabatic state is identified by subscript letters indicating the pair of monomers to which the charge transfer refers. (b) Comparison between diabatic state interactions ($V_e^{(1)}$ and $V_e^{(2)}$elements, see Figure 4) from (dashed) $\boldsymbol{mH}$ and (solid) the corresponding elements extracted from $\boldsymbol{H_{dia}}$.

To analyze the energy profiles of the adiabatic states in more detail and to identify the origin of CT mediated J-/H-aggregation [16,17,46] along the longitudinal translation coordinate, we expanded the exciton-state *wf*s of the trimer in terms of a set of symmetry-adapted diabatic functions defined by the linear combinations collected in Table S4. The $\boldsymbol{mH}$ off-diagonal matrix elements (FE/CT interactions), in the basis of the new *sdia* functions, (see Tables S5-S6) result to be proportional to the $\pm$ combinations of the D_e/D_h charge transfer integrals (see Figure 6a) as already seen for the dimer. Therefore, they display the same oscillatory profiles along the longitudinal translation shift which confers varying *sdia* contributions to each adiabatic state of the trimer. The modulation of the *wf* composition (in terms of *sdia*) can be appreciated in Figure 11, where the square coefficients of the FE/CT *sdia* contributions to the

adiabatic $1B_u$ state are reported along the longitudinal translation coordinate. The $1B_u$ *wf* is dominated by the *sdia* $CT1^{-+}$, FE^{-+} (see Table S4 for the labelling) in the range of 0.0 – 1.5 Å shifts but switches abruptly to the $CT1^{++}$, FE^{++} pair in the interval 2.0-3.0 Å, then it switches back to the pair $CT1^{-+}$, FE^{-+} in the range 4.0-6.0 Å and finally it reverts to the pair $CT1^{++}$, FE^{++} from 6.5 to 8.0 Å. Interestingly, similarly to the dimer, [33,45] the CT character of the $1B_u$ state is lower than 50% for the entire set of translational configurations and the contribution of the FE^{++} *sdia* function, in which the monomer transition dipole moments sum up, matches almost perfectly the evolution of the TD-ωB97XD/6-31G* computed transition dipole moment in Figure 7c. The role of CT-mediation in changing the H- to J- character of the trimer, when moving from 1.5 Å to 2.0 Å and from 6.0 to 6.5 Å longitudinal shifts, (Figure 7a) can be traced back to the *wf* composition of the $1B_u$ state switching from the pair of $CT1^{-+}$, FE^{-+} to the pair of $CT1^{++}$, FE^{++} functions (see Figure 11). In particular, the interchange of FE^{-+} and FE^{++} contributions to the *wf* is reflected in the change from H- to J- spectroscopic character and it is directly driven by the modulation of CT/FE interactions. Similarly, the varying *sdia* composition of the $1B_u$ adiabatic state is reflected in its energy profile (see Figure S8 where *sdia* energy profiles are also shown), whose trend is determined by the oscillating magnitude of the interactions between CT/FE *sdia* pairs along the longitudinal shift. A similar effect is clearly seen also for the pair of $1A_g - 3A_g$ adiabatic states of the trimer (see Figure 8a and Figure S8) whose energy profiles, modulated by the CT/FE *sdia* interactions, are almost specular with respect to those of the *sdia* states ($FE^{-}, CT1^{--}, CT1^{+-}$) dominating the two eigenstates. For the same reason, the *wf* compositions of the $1A_g - 3A_g$ adiabatic states are almost complementary for each geometrical configuration along the longitudinal shift (Figure S9).

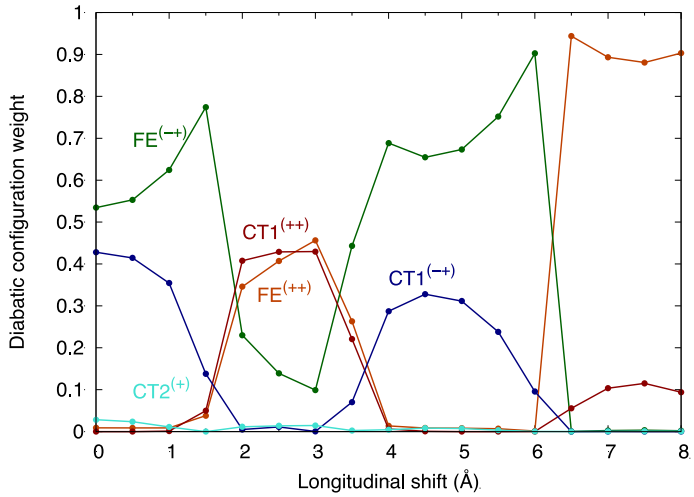

Figure 11. The *wf* composition of the adiabatic lowest exciton state ($1B_u$) of PBI trimer, in terms of the symmetry-adapted diabatic states defined in Table S4.

Concluding remarks.

Studying the effect of interchromophore rearrangements on exciton states of large aggregates may become an unaffordable task because of the high computational cost. To overcome this problem, in this work we have proposed to build a ***mH*** for large aggregates, based on QC calculations limited to the composing dimers. An exciton character analysis procedure is applied to the dimers and is used to generate the Hamiltonian representation $\boldsymbol{H_{dia}}$ on a diabatic basis chosen to coincide with the *LEs* built within a minimal monomer orbital space. The elements of $\boldsymbol{H_{dia}}$ obtained from the dimers that compose larger aggregates, are then used to build the ***mH*** whose diagonalization provides excitation energies and CT/FE exciton state character. The procedure is applied to trimers and tetramers of PBI for a series of geometrical configurations along the longitudinal translation coordinate, using TD-ωB97XD/6-31G* for the dimer calculations. To assess the quality of the cost-effective approach, we have also obtained the exciton states of the same systems from full-aggregate TD-ωB97XD/6-31G* calculations and analyzed their CT/FE character with the same diabatization protocol used for the dimers.

The comparison between the two approaches indicates limited deviations of the less expensive ***mH*** approach that can be ascribed to the approximations used to define the ***mH*** matrix elements. In all cases, the quality of the full-aggregate TD-ωB97XD/6-31G* calculations is retained at the ***mH*** level, not only for adiabatic excitation energies but also as regard the dominant CT/FE character of each eigenstate. In addition, along the longitudinal translation coordinate, both approaches predict an interchange of the H-/J- spectroscopic character for trimer and tetramer in agreement with the well-established interchange determined for dimers of PBI.

The simple form of the ***mH*** matrix elements has allowed to analyze in more detail the sequential change of the H-/J- character of the investigated PBI aggregates. The analysis in terms of a suitable symmetry-adapted diabatic basis, shows indeed that the most relevant CT/FE interactions are proportional to the combinations $D_e \pm D_h$ of charge transfer integrals, not only for the dimer but also for the trimer. The modulation of these interactions along the longitudinal translation coordinate allows to rationalize, for the trimer, the abrupt change in *wf* composition of the lowest energy adiabatic exciton state which, in turn, triggers the H- to J- character change for small longitudinal shifts. The analysis of adiabatic states in terms of symmetry-adapted diabatic states discloses therefore the role of CT-mediation governing the H-/J- character interchange along the longitudinal translation.

Summarizing, the ***mH*** approach proposed in this work, based on dimer calculations, can be considered a suitable alternative for the study of large chromophore aggregates since it provides results comparable to full-aggregate calculations at a fraction of the cost, meanwhile enabling a simple rationalization of the CT contribution to the photophysical character of the aggregate.

DATA AVAILABILITY

The data that supports the findings of this study are available within the article [and its supplementary material].

SUPPLEMENTARY MATERIAL

See the supplementary material for tables including the definition of symmetry-adapted diabatic basis and ***mH*** matrix elements on these bases and figures including details on the adiabatic excitation energy profiles, CT/FE character and *wf* composition.

AUTHOR INFORMATION

Corresponding Author

*Email: fabrizia.negri@unibo.it

ACKNOWLEDGMENT

RFO funds from the University of Bologna and computational resources from CINECA through an ISCRA (Italian Super Computing Resource Allocation) C project are acknowledged. Y. D. acknowledges MIUR for her PhD fellowship.

REFERENCES

[1] O. Ostroverkhova, *Organic Optoelectronic Materials: Mechanisms and Applications*, Chem. Rev. **116**, 13279 (2016).

[2] Y. Xu, P. Xu, D. Hu, and Y. Ma, *Recent Progress in Hot Exciton Materials for Organic Light-Emitting Diodes*, Chem. Soc. Rev. (2021).

[3] P. Yu, Y. Zhen, H. Dong, and W. Hu, *Crystal Engineering of Organic Optoelectronic Materials*, Chem **5**, 2814 (2019).

[4] F. Würthner, C. R. Saha-Möller, B. Fimmel, S. Ogi, P. Leowanawat, and D. Schmidt, *Perylene Bisimide Dye Assemblies as Archetype Functional Supramolecular Materials*,

Chem. Rev. **116**, 962 (2016).

[5] M. Hecht and F. Würthner, *Supramolecularly Engineered J-Aggregates Based on Perylene Bisimide Dyes*, Acc. Chem. Res. acs. accounts.0c00590 (2020).

[6] R. Haldar, A. Mazel, R. Joseph, M. Adams, I. A. Howard, B. S. Richards, M. Tsotsalas, E. Redel, S. Diring, F. Odobel, and C. Wöll, *Excitonically Coupled States in Crystalline Coordination Networks*, Chem. - A Eur. J. **23**, 14316 (2017).

[7] F. J. M. Hoeben, P. Jonkheijm, E. W. Meijer, and A. P. H. J. Schenning, *About Supramolecular Assemblies of Pi-Conjugated Systems.*, Chem. Rev. **105**, 1491 (2005).

[8] F. Su, G. Chen, P. A. Korevaar, F. Pan, H. Liu, Z. Guo, A. P. H. J. Schenning, H. Zhang, J. Lin, and Y. Jiang, *Discrete π-Stacks from Self-Assembled Perylenediimide Analogues.*, Angew. Chem. Int. Ed. Engl. **58**, 15273 (2019).

[9] L. Yang, P. Langer, E. S. Davies, M. Baldoni, K. Wickham, N. A. Besley, E. Besley, and N. R. Champness, *Synthesis and Characterisation of Rylene Diimide Dimers Using Molecular Handcuffs*, Chem. Sci. **10**, 3723 (2019).

[10] C. Kaufmann, D. Bialas, M. Stolte, and F. Würthner, *Discrete π-Stacks of Perylene Bisimide Dyes within Folda-Dimers: Insight into Long- and Short-Range Exciton Coupling*, J. Am. Chem. Soc. **140**, 9986 (2018).

[11] C. Kaufmann, W. Kim, A. Nowak-Król, Y. Hong, D. Kim, and F. Würthner, *Ultrafast Exciton Delocalization, Localization, and Excimer Formation Dynamics in a Highly Defined Perylene Bisimide Quadruple π-Stack*, J. Am. Chem. Soc. **140**, 4253 (2018).

[12] S. Samanta and D. Chaudhuri, *Suppressing Excimers in H-Aggregates of Perylene Bisimide Folda-Dimer: Role of Dimer Conformation and Competing Assembly*

Pathways, J. Phys. Chem. Lett. **8**, 3427 (2017).

[13] Y. Hong, J. Kim, W. Kim, C. Kaufmann, H. Kim, F. Würthner, and D. Kim, *Efficient Multiexciton State Generation in Charge-Transfer-Coupled Perylene Bisimide Dimers via Structural Control*, J. Am. Chem. Soc. **142**, 7845 (2020).

[14] R. Haldar, A. Mazel, M. Krstić, Q. Zhang, M. Jakoby, I. A. Howard, B. S. Richards, N. Jung, D. Jacquemin, S. Diring, W. Wenzel, F. Odobel, and C. Wöll, *A de Novo Strategy for Predictive Crystal Engineering to Tune Excitonic Coupling*, Nat. Commun. **10**, 2048 (2019).

[15] F. C. Spano, *The Spectral Signatures of Frenkel Polarons in H- and J-Aggregates*, Acc. Chem. Res. **43**, 429 (2010).

[16] N. J. Hestand and F. C. Spano, *Molecular Aggregate Photophysics beyond the Kasha Model: Novel Design Principles for Organic Materials*, Acc. Chem. Res. **50**, 341 (2017).

[17] N. J. Hestand and F. C. Spano, *Expanded Theory of H- and J-Molecular Aggregates: The Effects of Vibronic Coupling and Intermolecular Charge Transfer*, Chem. Rev. **118**, 7069 (2018).

[18] R. E. Cook, B. T. Phelan, R. J. Kamire, M. B. Majewski, R. M. Young, and M. R. Wasielewski, *Excimer Formation and Symmetry-Breaking Charge Transfer in Cofacial Perylene Dimers*, J. Phys. Chem. A **121**, 1607 (2017).

[19] A. Schubert, V. Settels, W. Liu, F. Würthner, C. Meier, R. F. Fink, S. Schindlbeck, S. Lochbrunner, B. Engels, and V. Engel, *Ultrafast Exciton Self-Trapping upon Geometry Deformation in Perylene-Based Molecular Aggregates*, J. Phys. Chem. Lett. **4**, 792

(2013).

[20] M. Deutsch, S. Wirsing, D. Kaiser, R. F. Fink, P. Tegeder, and B. Engels, *Geometry Relaxation-Mediated Localization and Delocalization of Excitons in Organic Semiconductors: A Quantum Chemical Study*, J. Chem. Phys. **153**, 224104 (2020).

[21] E. A. Margulies, J. L. Logsdon, C. E. Miller, L. Ma, E. Simonoff, R. M. Young, G. C. Schatz, and M. R. Wasielewski, *Direct Observation of a Charge-Transfer State Preceding High-Yield Singlet Fission in Terrylenediimide Thin Films*, J. Am. Chem. Soc. **139**, 663 (2017).

[22] E. A. Margulies, C. E. Miller, Y. Wu, L. Ma, G. C. Schatz, R. M. Young, and M. R. Wasielewski, *Enabling Singlet Fission by Controlling Intramolecular Charge Transfer in π-Stacked Covalent Terrylenediimide Dimers*, Nat. Chem. **8**, 1120 (2016).

[23] R. M. Young and M. R. Wasielewski, *Mixed Electronic States in Molecular Dimers: Connecting Singlet Fission, Excimer Formation, and Symmetry-Breaking Charge Transfer*, Acc. Chem. Res. **53**, 1957 (2020).

[24] D. Beljonne, H. Yamagata, J. L. Brédas, F. C. Spano, and Y. Olivier, *Charge-Transfer Excitations Steer the Davydov Splitting and Mediate Singlet Exciton Fission in Pentacene*, Phys. Rev. Lett. **110**, 226402 (2013).

[25] T. C. Berkelbach, M. S. Hybertsen, and D. R. Reichman, *Microscopic Theory of Singlet Exciton Fission. II. Application to Pentacene Dimers and the Role of Superexchange*, J. Chem. Phys. **138**, 114103 (2013).

[26] T. Zeng, R. Hoffmann, and N. Ananth, *The Low-Lying Electronic States of Pentacene and Their Roles in Singlet Fission*, J. Am. Chem. Soc. **136**, 5755 (2014).

[27] D. Casanova, *Theoretical Modeling of Singlet Fission*, Chem. Rev. **118**, 7164 (2018).

[28] G. Han and Y. Yi, *Local Excitation/Charge-Transfer Hybridization Simultaneously Promotes Charge Generation and Reduces Nonradiative Voltage Loss in Nonfullerene Organic Solar Cells*, J. Phys. Chem. Lett. **10**, 2911 (2019).

[29] V. Coropceanu, X.-K. Chen, T. Wang, Z. Zheng, and J.-L. Brédas, *Charge-Transfer Electronic States in Organic Solar Cells*, Nat. Rev. Mater. **4**, 689 (2019).

[30] S. A. Mewes and A. Dreuw, *Density-Based Descriptors and Exciton Analyses for Visualizing and Understanding the Electronic Structure of Excited States*, Phys. Chem. Chem. Phys. **21**, 2843 (2019).

[31] S. A. Mewes, F. Plasser, A. Krylov, and A. Dreuw, *Benchmarking Excited-State Calculations Using Exciton Properties*, J. Chem. Theory Comput. **14**, 710 (2018).

[32] S. Jurinovich, L. Cupellini, C. A. Guido, and B. Mennucci, *EXAT: EXcitonic Analysis Tool*, J. Comput. Chem. **39**, 279 (2018).

[33] C. Walter, V. Krämer, and B. Engels, *On the Applicability of Time-Dependent Density Functional Theory (TDDFT) and Semiempirical Methods to the Computation of Excited-State Potential Energy Surfaces of Perylene-Based Dye-Aggregates*, Int. J. Quantum Chem. **117**, e25337 (2017).

[34] D. Accomasso, M. Persico, and G. Granucci, *Diabatization by Localization in the Framework of Configuration Interaction Based on Floating Occupation Molecular Orbitals (FOMO−CI)*, ChemPhotoChem **3**, 933 (2019).

[35] H. Tamura, *Diabatization for Time-Dependent Density Functional Theory: Exciton Transfers and Related Conical Intersections*, J. Phys. Chem. A **120**, 9341 (2016).

[36] W. Liu, B. Lunkenheimer, V. Settels, B. Engels, R. F. Fink, and A. Köhn, *A General Ansatz for Constructing Quasi-Diabatic States in Electronically Excited Aggregated Systems*, J. Chem. Phys. **143**, 084106 (2015).

[37] A. Carreras, O. Uranga-Barandiaran, F. Castet, and D. Casanova, *Photophysics of Molecular Aggregates from Excited State Diabatization*, J. Chem. Theory Comput. **15**, 2320 (2019).

[38] S. Shirai, S. Iwata, T. Tani, and S. Inagaki, *Ab Initio Studies of Aromatic Excimers Using Multiconfiguration Quasi-Degenerate Perturbation Theory*, J. Phys. Chem. A **115**, 7687 (2011).

[39] A. A. M. H. M. Darghouth, G. C. Correa, S. Juillard, M. E. Casida, A. Humeniuk, and R. Mitrić, *Davydov-Type Excitonic Effects on the Absorption Spectra of Parallel-Stacked and Herringbone Aggregates of Pentacene: Time-Dependent Density-Functional Theory and Time-Dependent Density-Functional Tight Binding*, J. Chem. Phys. **149**, 134111 (2018).

[40] D. Casanova, *Theoretical Investigations of the Perylene Electronic Structure: Monomer, Dimers, and Excimers*, Int. J. Quantum Chem. **115**, 442 (2015).

[41] M. Zubiria-Ulacia, J. M. Matxain, and D. Casanova, *The Role of CT Excitations in PDI Aggregates*, Phys. Chem. Chem. Phys. **22**, 15908 (2020).

[42] Y. Mao, A. Montoya-Castillo, and T. E. Markland, *Accurate and Efficient DFT-Based Diabatization for Hole and Electron Transfer Using Absolutely Localized Molecular Orbitals*, J. Chem. Phys. **151**, 164114 (2019).

[43] Y. Mao, A. Montoya-Castillo, and T. E. Markland, *Excited State Diabatization on the*

Cheap Using DFT: Photoinduced Electron and Hole Transfer, J. Chem. Phys. **153**, 244111 (2020).

[44] C. J. Bardeen, *The Structure and Dynamics of Molecular Excitons*, Annu. Rev. Phys. Chem. **65**, 127 (2014).

[45] W. Liu, S. Canola, A. Köhn, B. Engels, F. Negri, and R. F. Fink, *A Model Hamiltonian Tuned toward High Level Ab Initio Calculations to Describe the Character of Excitonic States in Perylenebisimide Aggregates*, J. Comput. Chem. **39**, 1979 (2018).

[46] A. Oleson, T. Zhu, I. S. Dunn, D. Bialas, Y. Bai, W. Zhang, M. Dai, D. R. Reichman, R. Tempelaar, L. Huang, and F. C. Spano, *Perylene Diimide-Based Hj- and HJ-Aggregates: The Prospect of Exciton Band Shape Engineering in Organic Materials*, J. Phys. Chem. C **123**, 20567 (2019).

[47] J. Seibt and V. Engel, *Absorption and Emission Spectroscopy of Molecular Trimers: Cyclic versus Linear Geometries*, Chem. Phys. **347**, 120 (2008).

[48] J. Seibt, T. Winkler, K. Renziehausen, V. Dehm, F. Würthner, H.-D. Meyer, and V. Engel, *Vibronic Transitions and Quantum Dynamics in Molecular Oligomers: A Theoretical Analysis with an Application to Aggregates of Perylene Bisimides.*, J. Phys. Chem. A **113**, 13475 (2009).

[49] M. Schröter, S. D. Ivanov, J. Schulze, S. P. Polyutov, Y. Yan, T. Pullerits, and O. Kühn, *Exciton–Vibrational Coupling in the Dynamics and Spectroscopy of Frenkel Excitons in Molecular Aggregates*, Phys. Rep. **567**, 1 (2015).

[50] D. Bialas, C. Zhong, F. Würthner, and F. C. Spano, *Essential States Model for Merocyanine Dye Stacks: Bridging Electronic and Optical Absorption Properties*, J.

Phys. Chem. C **123**, 18654 (2019).

[51] B. Shi, D. Nachtigallová, A. J. A. Aquino, F. B. C. Machado, and H. Lischka, *Excited States and Excitonic Interactions in Prototypic Polycyclic Aromatic Hydrocarbon Dimers as Models for Graphitic Interactions in Carbon Dots*, Phys. Chem. Chem. Phys. **21**, 9077 (2019).

[52] H. Fliegl, Z. You, C. Hsu, and D. Sundholm, *The Excitation Spectra of Naphthalene Dimers: Frenkel and Charge-transfer Excitons*, J. Chinese Chem. Soc. **63**, 20 (2016).

[53] W. Liu, V. Settels, P. H. P. Harbach, A. Dreuw, R. F. Fink, and B. Engels, *Assessment of TD-DFT- and TD-HF-Based Approaches for the Prediction of Exciton Coupling Parameters, Potential Energy Curves, and Electronic Characters of Electronically Excited Aggregates*, J. Comput. Chem. **32**, 1971 (2011).

[54] V. Settels, W. Liu, J. Pflaum, R. F. Fink, and B. Engels, *Comparison of the Electronic Structure of Different Perylene-Based Dye-Aggregates.*, J. Comput. Chem. **33**, 1544 (2012).

[55] A. Mukazhanova, W. Malone, H. Negrin-Yuvero, S. Fernandez-Alberti, S. Tretiak, and S. Sharifzadeh, *Photoexcitation Dynamics in Perylene Diimide Dimers*, J. Chem. Phys. **153**, 244117 (2020).

[56] D. Bellinger, J. Pflaum, C. Brüning, V. Engel, and B. Engels, *The Electronic Character of PTCDA Thin Films in Comparison to Other Perylene-Based Organic Semi-Conductors: Ab Initio-, TD-DFT and Semi-Empirical Computations of the Opto-Electronic Properties of Large Aggregates*, Phys. Chem. Chem. Phys. **19**, 2434 (2017).

[57] B. Engels and V. Engel, *The Dimer-Approach to Characterize Opto-Electronic*

Properties of and Exciton Trapping and Diffusion in Organic Semiconductor Aggregates and Crystals, Phys. Chem. Chem. Phys. **19**, 12604 (2017).

[58] S. J. Jang and B. Mennucci, *Delocalized Excitons in Natural Light-Harvesting Complexes*, Rev. Mod. Phys. **90**, 035003 (2018).

[59] A. Hellweg, S. A. Grün, and C. Hättig, *Benchmarking the Performance of Spin-Component Scaled CC2 in Ground and Electronically Excited States*, Phys. Chem. Chem. Phys. **10**, 4119 (2008).

[60] N. O. C. Winter, N. K. Graf, S. Leutwyler, and C. Hättig, *Benchmarks for 0–0 Transitions of Aromatic Organic Molecules: DFT/B3LYP, ADC(2), CC2, SOS-CC2 and SCS-CC2 Compared to High-Resolution Gas-Phase Data*, Phys. Chem. Chem. Phys. **15**, 6623 (2013).

[61] A. Dreuw and M. Wormit, *The Algebraic Diagrammatic Construction Scheme for the Polarization Propagator for the Calculation of Excited States*, Wiley Interdiscip. Rev. Comput. Mol. Sci. **5**, 82 (2015).

[62] A. A. Kocherzhenko, X. A. Sosa Vazquez, J. M. Milanese, and C. M. Isborn, *Absorption Spectra for Disordered Aggregates of Chromophores Using the Exciton Model*, J. Chem. Theory Comput. **13**, 3787 (2017).

[63] A. A. Kocherzhenko, S. V. Shedge, X. Sosa Vazquez, J. Maat, J. Wilmer, A. F. Tillack, L. E. Johnson, and C. M. Isborn, *Unraveling Excitonic Effects for the First Hyperpolarizabilities of Chromophore Aggregates*, J. Phys. Chem. C **123**, 13818 (2019).

[64] A. A. Kocherzhenko, S. V. Shedge, P. F. Germaux, M. Heidarian, and C. M. Isborn, *Excitonic Hamiltonians for Calculating Optical Absorption Spectra and Optoelectronic*

Properties of Molecular Aggregates and Solids, J. Vis. Exp. (2020).

[65] X. Li, R. M. Parrish, F. Liu, S. I. L. Kokkila Schumacher, and T. J. Martínez, *An Ab Initio Exciton Model Including Charge-Transfer Excited States*, J. Chem. Theory Comput. **13**, 3493 (2017).

[66] A. Sisto, C. Stross, M. W. van der Kamp, M. O'Connor, S. McIntosh-Smith, G. T. Johnson, E. G. Hohenstein, F. R. Manby, D. R. Glowacki, and T. J. Martinez, *Atomistic Non-Adiabatic Dynamics of the LH2 Complex with a GPU-Accelerated Ab Initio Exciton Model*, Phys. Chem. Chem. Phys. **19**, 14924 (2017).

[67] X. Li, R. M. Parrish, and T. J. Martínez, *An Ab Initio Exciton Model for Singlet Fission*, J. Chem. Phys. **153**, 184116 (2020).

[68] S. Jiang, Y. Xie, and Z. Lan, *The Role of the Charge-Transfer States in the Ultrafast Excitonic Dynamics of the DTDCTB Dimers Embedded in a Crystal Environment*, Chem. Phys. **515**, 603 (2018).

[69] P. Petelenz, *Mixing of Frenkel Excitons with Charge Transfer States in the Neighbourhood of Charged Defect*, Chem. Phys. Lett. **47**, 603 (1977).

[70] J. E. Norton and J.-L. Brédas, *Theoretical Characterization of Titanyl Phthalocyanine as a P-Type Organic Semiconductor: Short Intermolecular Π-π Interactions Yield Large Electronic Couplings and Hole Transport Bandwidths*, J. Chem. Phys. **128**, 034701 (2008).

[71] D. Kim, *A Theoretical Analysis of the Excited State of Oligoacene Aggregates: Local Excitation vs. Charge-Transfer Transition*, Bull. Korean Chem. Soc. **36**, 2284 (2015).

[72] P. Löwdin, *On the Non-Orthogonality Problem Connected with the Use of Atomic Wave*

Functions in the Theory of Molecules and Crystals, J. Chem. Phys. **18**, 365 (1950).

[73] Å. Björck, *Numerics of Gram-Schmidt Orthogonalization*, Linear Algebra Appl. **197**–**198**, 297 (1994).

[74] M. Nottoli, S. Jurinovich, L. Cupellini, A. T. Gardiner, R. Cogdell, and B. Mennucci, *The Role of Charge-Transfer States in the Spectral Tuning of Antenna Complexes of Purple Bacteria*, Photosynth. Res. **137**, 215 (2018).

[75] D. Casanova and A. I. Krylov, *Quantifying Local Exciton, Charge Resonance, and Multiexciton Character in Correlated Wave Functions of Multichromophoric Systems*, J. Chem. Phys. **144**, 014102 (2016).

[76] M. B. Smith and J. Michl, *Singlet Fission*, Chem. Rev. **110**, 6891 (2010).

[77] A. Szabo and N. Ostlund, *Modern Quantum Chemistry : Introduction to Advanced Electronic Structure Theory*, Dover Publications, Inc., New York, 1996, 1st ed.

[78] V. Coropceanu, J. Cornil, D. A. da Silva Filho, Y. Olivier, R. Silbey, and J.-L. Brédas, *Charge Transport in Organic Semiconductors*, Chem. Rev. **107**, 926 (2007).

[79] E. Di Donato, R. P. Fornari, S. Di Motta, Y. Li, Z. Wang, and F. Negri, *N-Type Charge Transport and Mobility of Fluorinated Perylene Bisimide Semiconductors.*, J. Phys. Chem. B **114**, 5327 (2010).

[80] S. Canola and F. Negri, *Role of the HOMO-1 Orbital on the p-Type Charge Transport of the Fused-Ring Thienoacene DBTDT*, J. Phys. Chem. C **119**, (2015).

[81] S. Canola, C. Graham, Á. J. Pérez-Jiménez, J. C. Sancho-García, and F. Negri, *Charge Transport Parameters for Carbon Based Nanohoops and Donor-Acceptor Derivatives*,

Phys. Chem. Chem. Phys. **21**, 2057 (2019).

[82] R. F. Fink, J. Seibt, V. Engel, M. Renz, M. Kaupp, S. Lochbrunner, H.-M. Zhao, J. Pfister, F. Würthner, and B. Engels, *Exciton Trapping in Pi-Conjugated Materials: A Quantum-Chemistry-Based Protocol Applied to Perylene Bisimide Dye Aggregates.*, J. Am. Chem. Soc. **130**, 12858 (2008).

[83] M. J. Frisch, G. W. Trucks, H. E. Schlegel, G. E. Scuseria, M. A. Robb, J. R. Cheeseman, G. Scalmani, V. Barone, G. A. Petersson, F. O., J. B. Foresman, and J. D. Fox, *Gaussian 16*, Gaussian, Inc., Wallingford CT,.

[84] N. J. Hestand, R. V. Kazantsev, A. S. Weingarten, L. C. Palmer, S. I. Stupp, and F. C. Spano, *Extended-Charge-Transfer Excitons in Crystalline Supramolecular Photocatalytic Scaffolds*, J. Am. Chem. Soc. **138**, 11762 (2016).

[85] V. Stehr, B. Engels, C. Deibel, and R. F. Fink, *Anisotropy of Singlet Exciton Diffusion in Organic Semiconductor Crystals from Ab Initio Approaches*, J. Chem. Phys. **140**, 024503 (2014).

[86] D. Bellinger, V. Settels, W. Liu, R. F. Fink, and B. Engels, *Influence of a Polarizable Surrounding on the Electronically Excited States of Aggregated Perylene Materials*, J. Comput. Chem. **37**, 1601 (2016).